PERGAMON

International Journal of Heat and Mass Transfer 45 (2002) 4021–4031

International Journal of HEAT and MASS TRANSFER

www.elsevier.com/locate/ijhmt

Laminar free convection underneath a hot horizontal infinite flat strip

A. Dayan *, R. Kushnir, A. Ullmann

Department of Fluid Mechanics and Heat Transfer, Faculty of Engineering, Tel Aviv University, Ramat Aviv, 69978 Tel Aviv, Israel

Received 26 January 2001; received in revised form 1 December 2001

Abstract

Analyses were conducted to study the problem of natural convection underneath a hot and isothermal horizontal infinite flat strip. It included a numerical and an analytical investigation of the problem. The work offers simple closed form solutions for the critical flow depth, boundary layer thickness and heat transfer coefficient. The governing equations were solved by the integral method. The justification for applying self-similar boundary layer profiles was demonstrated both numerically and from analyses of published experimental results. The solution was improved through the use of numerical analyses as well as from analytical inspection of limiting cases. The results were successfully tested against published experimental data. Furthermore, the work offers an explanation for the discrepancy that exists amongst the various heat transfer correlations found in the literature.

1. Introduction

An investigation of the problem of free convection underneath a hot and isothermal horizontal infinite flat strip is presented. Previous studies revealed that buoyancy forces induce a flow from the strip center toward the strip edges [1,2]. It was demonstrated that, in a practical sense, the flow near the surface exhibits boundary layer characteristics along most of the strip width. The ambient airflow rises from below upwards and towards the strip center. At a certain distance from the strip the airflow reverses its lateral direction and flows towards the strip edge (see Figs. 1 and 3). The points of flow reversal form a virtual surface that represents a boundary where the flow lacks any lateral velocity component. The flow confined between this boundary and the strip surface moves towards the strip edges. As mentioned, this flow exhibits boundary layer characteristics. While picking up heat, it accelerates as it moves towards the two strip edges. The boundary layer is thickest at the strip center and thinnest at the edges. The thickness at the edge is determined from critical flow conditions which, in principle, indicate that the flow reaches its maximal velocity before leaving the strip edge (from the conversion of potential energy to kinetic energy for conditions of negligible downstream flow resistance).

The current work focuses on the modeling of the boundary layer for laminar flow conditions. Several investigators, interested in the cooling of flat plates and strips, have previously studied this subject. Correlations for the heat transfer coefficient were developed numerically, analytically and empirically. Most of the correlations are of the form

$$\overline{Nu}_L = CRa_L^{1/5}, \quad \text{for laminar flow} \tag{1}$$

where $\overline{Nu}_L$ is the averaged Nusselt number, Ra_L the Rayleigh number, the subscript L denotes a characteristic length L (half the strip width), and C is a coefficient that depends on the Prandtl number. All properties are calculated at the mean temperature between the surface and the ambient temperatures. Comparison of the correlations, however, reveals inconsistencies in the proposed values of C. Those discrepancies are investigated in the current work. In this context, Aihara et al. [1] investigated experimentally a two-dimensional airflow underneath a rectangular plate (25 cm wide). To portray

* Corresponding author.

0017-9310/02/$ - see front matter
PII: S0017-9310(02)00116-3

Nomenclature

A, B	coefficients, Eq. (16)
C	coefficient, Eq. (1)
F	hypergeometric function
f_i	$i = 1$–8, Eqs. (5a), (5b) and (9)
g	gravitational acceleration
h_y	local heat transfer coefficient
$\overline{h}$	average heat transfer coefficient
k	thermal conductivity
L	strip half width
L^*	dimensionless length, $L/\sqrt[3]{\alpha v/g}$
$\dot{M}$	mass discharge rate
Nu_y	local Nusselt number, $h_y y/k$
$\overline{Nu}_L$	average Nusselt number, $\overline{h}L/k$
P	pressure
Pr	Prandtl number, v/α
$\dot{Q}$	energy rate
Ra_L	Rayleigh number, $g\beta L^3\theta_w/\alpha v$
T	temperature
u	specific internal energy
$\dot{U}$	specific internal energy flux
V	characteristic velocity
V^*	dimensionless velocity
v, w	horizontal and vertical velocity components
y, z	horizontal and vertical coordinate axes

Greek symbols

α	thermal diffusivity
β	thermal expansion coefficient
Γ	gamma function
δ	boundary layer depth
δ_C	critical depth at the stripe edge
δ_t	thermal boundary layer depth
η	dimensionless coordinate, z/δ
v	kinematic viscosity
Θ	dimensionless temperature
θ	temperature difference $(T - T_\infty)$
ρ	density

Subscripts

w	wall conditions
∞	ambient conditions
ref	reference value

the two-dimensional flow characteristics underneath a strip, they bounded the plate by two vertical sidewalls. Based on their experiments they proposed empirical values of $C = 0.5$ for $Ra_L = 7.16 \times 10^6$ and $C = 0.509$ for $Ra_L = 1.02 \times 10^7$. In their work, velocity and temperature profiles were measured by tracers' photography and with thermocouples, respectively. They argue that, in a true sense, self-similar profiles do not develop underneath horizontal plates. However, their investigation indicated that it is possible to define a boundary layer zone with characteristic temperature and velocity profiles for integral method analyses. They demonstrated that such profiles approximate fairly well the measured data along most of the plate length. This was an important conclusion since most subsequent analyses incorporated the integral solution method. The success of the method is contingent on the existence of similarity in boundary layer velocity and temperature profiles. In the current work, it is demonstrated, however, that the assumption on the existence of self-similar profile is more warranted than what was claimed in Aihara's work.

Fuji and Imura [2], conducted experiments with horizontal and tilted plates in water ($Pr > 1$). The plates were bounded, as in Aihara's investigation, to induce two-dimensional strip like flows. From measured wall heat transfer coefficients (for horizontal surfaces) they proposed a value of $C = 0.44$, for Rayleigh numbers between 10^6 and 10^{11}. This value is based on a particular weighted average of fluid properties. A regular averaging calculation would have produced a higher value (for a representative single point calculation we obtained $C = 0.48$). For free convection along vertical walls, conducted by the same investigators, their averaging method produced, again, lower values of C as compared to those of well-established correlations (about 7% smaller).

The integral method was also incorporated for the study of an infinite isothermal strip by Wagner [3] and Singh et al. [4]. For a zero boundary layer thickness at the strip edges, both calculated a coefficient of $C = 0.5$ for Prandtl number of the order of 1. Singh and Birbank [5] expanded the integral method to allow for a finite boundary layer thickness at the strip edges and evaluated numerically a value of $C = 0.46$ for $Pr = 0.7$. Similarly, Clifton and Chapman [6] also applied the integral method to solve the problem but for a boundary condition of critical flow at the strip edge. They solved the integral equations numerically and obtained $C = 0.44$ for $Pr = 0.7$. Furthermore, by neglecting inertia terms they developed an approximate close form solution suggesting that $C = 0.49$ for $Pr = 0.7$.

Goldstein and Lau [7] solved numerically by a finite difference method the two-dimensional problem including the external circulatory flow pattern. Their analyses were for small Rayleigh numbers ranging from 40 to 8000 and for $Pr = 0.7$. They concluded that the flow and temperature profiles near the strip surface resemble those of typical boundary layers. They proposed a value of $C = 0.56$ and a power of 0.19 for the Rayleigh number (rather than 0.2). Higuera [8] combined an as-

ymptotic solution and numerical analyses to suggest a coefficient of $C = 0.442$, for $Pr = 0.7$.

Inspection of the above analyses clearly indicates that the proposed values of the coefficient C are scattered. No explanation could be found for the apparent discrepancies. One may argue, however, that different assumptions and solution approximations could be the cause for these inconsistencies. This refers, for instance, to the outcome of ignoring inertia terms or the assumption of zero boundary layer thickness at the strip edge. However, we did not dismiss the problem at this level, and went further to investigate and verify if a more fundamental cause could have been overlooked. We think that indeed this is the case. The reason found reconciles different results. It is presented and discussed in a subsequent section.

In general, the current work was undertaken with the purpose of developing an analytical solution that accounts, at least in part, for all the affecting parameters and reproduces quite accurately the experimental local Nusselt numbers. It is based on an improved representation of the critical flow boundary condition at the strip edges and accounts for inertia effects. Numerical analyses were conducted over a large range of Rayleigh numbers and strip widths. The numerical computations were used to analyze and validate the analytical solutions. Additionally, it is worth noting that the analytical approach can be considered as a simple and attractive solution method that can be incorporated for the analyses of a more complex hot surface geometry.

2. Analytical solution

Consider a horizontal isothermal hot flat strip facing down as shown in Fig. 1. The strip is insulated on its sides and above. For the indicated coordinate system, the momentum, continuity and energy equations subject to the boundary layer and Bousinesq approximations are:

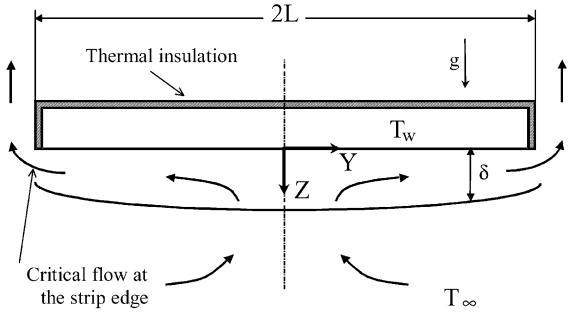

Fig. 1. Natural convection underneath a hot horizontal flat strip.

$$\left(v\frac{\partial v}{\partial y}+w\frac{\partial v}{\partial z}\right)=-\frac{1}{\rho}\frac{\partial p}{\partial y}+\nu\frac{\partial^2 v}{\partial z^2} \tag{2a}$$

$$\frac{\partial p}{\partial z}=\rho_\infty[1-\beta(T-T_\infty)]g \tag{2b}$$

$$\frac{\partial v}{\partial y}+\frac{\partial w}{\partial z}=0 \tag{2c}$$

and

$$v\frac{\partial T}{\partial y}+w\frac{\partial T}{\partial z}=\alpha\frac{\partial^2 T}{\partial z^2} \tag{2d}$$

This representation is valid for the range of $(\delta/L)^2 < 0.1$ and $Ra \times Pr > 10^5$ [6]. The boundary conditions for a constant wall temperature are:

$$\text{at } z=0, \quad v=w=0, \quad T=T_w \tag{3a}$$

$$\text{as } z\to\infty, \quad v=0, \quad \frac{\partial v}{\partial z}=0, \quad T=T_\infty, \quad \frac{\partial T}{\partial z}=0 \tag{3b}$$

and

$$\text{at } y=0, \quad v=0 \tag{3c}$$

For fluids with Prandtl numbers close to unity it is reasonable to assume that the momentum and the temperature boundary layers have an identical thickness δ.

The set of governing equations can be solved by the integral solution method if one assumes that the velocity and temperature profiles exhibit similarity characteristics. For natural convection problems, the integral solution method has been used before and proved to produce quite accurate results. Furthermore, the fact that similarity profiles are representative has been demonstrated in our numerical investigation (as presented in a later section).

To use the integral method, as previously mentioned, it is necessary to define velocity and temperature profiles. The profiles are often polynomials that satisfy the boundary conditions as well as the differential equations at the boundaries. Self similar velocity and temperature profiles are defined as

$$\frac{v}{V}=V^*(\eta) \tag{4a}$$

$$\frac{T-T_\infty}{T_w-T_\infty}=\frac{\theta}{\theta_w}=\Theta(\eta) \tag{4b}$$

where $\eta = z/\delta$ and V is a characteristic velocity that is y dependent only.

The substitution of the velocity and temperature profiles (4a) and (4b) into Eqs. (2a)–(2d) and integration across the boundary layer thickness, subject to the boundary conditions, yields

$$f_1\frac{\mathrm{d}(V^2\delta)}{\mathrm{d}y}+f_2 g\beta\theta_w\delta\frac{\mathrm{d}\delta}{\mathrm{d}y}+f_3\frac{\nu V}{\delta}=0 \tag{5a}$$

$$f_4 \frac{\mathrm{d}(V\delta)}{\mathrm{d}y} = f_5 \frac{\alpha}{\delta} \tag{5b}$$

where

$$f_1 = \int_0^1 V^{*^2}\,\mathrm{d}\eta, \quad f_2 = 2\int_0^1 \int_\eta^1 \Theta\,\mathrm{d}\eta'\,\mathrm{d}\eta,$$
$$f_3 = \left.\frac{\partial V^*}{\partial \eta}\right|_{\eta=0}, \quad f_4 = \int_0^1 V^*\Theta\,\mathrm{d}\eta, \quad f_5 = -\left.\frac{\partial \Theta}{\partial \eta}\right|_{\eta=0}$$

The boundary conditions at the strip center and at its edge are

$$\text{at } y = 0 \quad V = 0 \tag{6a}$$

$$\text{at } y = L \quad \delta = \delta_C \tag{6b}$$

where δ_C is the boundary layer thickness for critical flow conditions at the strip edge.

The conservation Eqs. (5a) and (5b) contain five terms, representing inertia, buoyancy, drag, convection, and conduction. From all five, the buoyancy term is the only one sensitive and completely dependent on the boundary layer shape, or alternatively to the longitudinal derivative of its thickness. Under a horizontal surface, if not for the boundary layer curvature, buoyancy would lack the capacity of driving a convection flow. In contrast, the curvature has little effects on all other terms. Based on, either, tests [9] or dimensional analyses, one can find that the boundary layer thickness is fairly uniform along most of the flow run. Applying these conclusions significantly simplified the solution of the equations. In contrast to previous investigations, in the current approach, effects of all the five derivatives are accounted for in the simplified equations.

For a nearly constant boundary layer thickness, the first-order approximation of the energy equation solution is

$$V = \frac{f_5 \alpha}{f_4 \delta^2} y \tag{7}$$

Substituting Eq. (7) for velocity terms of the momentum equation, and assuming a nearly constant boundary layer thickness (retaining the boundary layer thickness derivative only for the buoyancy term) yields the following first-order solution approximation

$$\delta = \left[\delta_C^5 + \frac{5\alpha^2 f_5 (2f_1 f_5 + f_3 f_4 Pr)}{2 f_2 f_4^2 g\beta\theta_w}\left(L^2 - y^2\right)\right]^{1/5} \tag{8}$$

The boundary layer thickness at the strip edge, δ_C, is calculated for critical flow conditions at that point. As seen from the solution, the fluid velocity increases as it approaches the strip edge. At the edge, the boundary layer assumes its minimal thickness. For critical flow conditions at the edge, this thickness provides a maximal mass discharge rate for the local fluid energy [10].

For half of the strip width, an energy transfer of $\dot{Q}/2$ enters the boundary layer and is convected out of the strip at its edge. This energy can be calculated by integration of the total enthalpy at the strip edge, for the velocity and temperature profiles Eqs. (4a) and (4b) subject to a variable air density in the buoyancy and pressure terms. The pressure is calculated according to Eq. (2b) for a reference value P_{ref} at a distance Z_{ref} below the strip (see Fig. 2). The integration of the total enthalpy at the strip edge per unit strip length is therefore

$$\begin{aligned}\frac{\dot{Q}}{2} &= \int_0^{\delta_C} \left(u + \frac{v^2}{2} - gz + \frac{P}{\rho}\right)\rho v\,\mathrm{d}z \\ &= \dot{U} + f_6\rho_\infty V^3\delta_C + f_8(V\delta_C P_{ref} - \rho_\infty V g Z_{ref}\delta_C) \\ &\quad + f_7\rho_\infty V g\beta\theta_w\delta_C^2\end{aligned} \tag{9}$$

where u and $\dot{U}$ represent the fluid specific internal energy and its flux at the strip edge, respectively and

$$f_6 = \frac{1}{2}\int_0^1 V^{*^3}\,\mathrm{d}\eta,$$
$$f_7 = \int_0^1 \left[\left(\int_\eta^1 \Theta\,\mathrm{d}\eta'\right)V^* + \Theta V^*\eta\right]\mathrm{d}\eta, \quad f_8 = \int_0^1 V^*\,\mathrm{d}\eta$$

The mass discharge rate at the strip edge per unit length is

$$\dot{M} = \int_0^{\delta_C} \rho v\,\mathrm{d}z = f_8\rho_\infty V\delta_C \tag{10}$$

Combining Eqs. (9) and (10), to identify $\dot{M}$, yields

$$\dot{U} + \frac{f_6\dot{M}^3}{f_8^3\rho_\infty^2\delta_C^2} + \frac{p_{ref}\dot{M}}{\rho_\infty} - gZ_{ref}\dot{M} + \frac{f_7 g\beta\theta_w\delta_C\dot{M}}{f_8} - \frac{\dot{Q}}{2} = 0 \tag{11}$$

Equating the derivative of Eq. (11) to zero enables the calculation of the maximum discharge rate $\dot{M}$ for an energy input $\dot{Q}/2$. This is done according to

$$\frac{\mathrm{d}\dot{M}}{\mathrm{d}\delta_C} = 0 \tag{12}$$

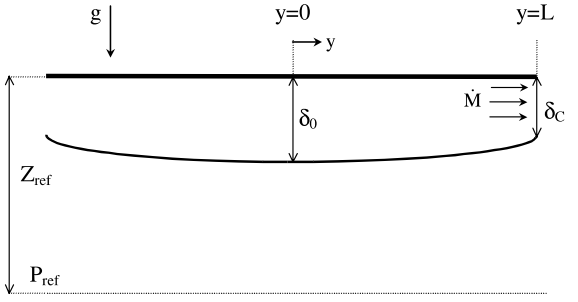

Fig. 2. Boundary layer schematics for the calculation of the critical depth.

Since most of the convected energy $\dot{Q}/2$ is in the thermal component $\dot{U}$, it is assumed that the derivative of their difference $(\dot{Q}/2 - \dot{U})$ with respect to δ_C is negligible. It implies that conditions of critical flow are dictated by how the mechanical energy redistributes itself among the pressure, the kinetic and the potential components at the point of discharge. With this assumption, the critical flow was found to be

$$\delta_C = \left(\frac{2 f_6 \dot{M}^2}{f_7 f_8^2 \rho_\infty^2 g \beta \theta_w} \right)^{1/3} \tag{13}$$

Substitution of Eq. (10) yields

$$\delta_C = \left(\frac{2 f_5^2 f_6 \alpha^2 L^2}{f_4^2 f_7 g \beta \theta_w} \right)^{1/5} \tag{14}$$

It is well known that in open channels the critical depth occurs at about $2\delta_C$ upstream the channel edge [11]. It is thus common to estimate the fluid depth at the channel edge to be somewhat smaller than the theoretical critical depth. It is reasonable to apply that assumption for the horizontal strip critical flow as well. We therefore assumed that the boundary layer critical thickness at the strip edges equals $0.9\delta_C$, or

$$\begin{aligned} \delta &= \left[\frac{2 f_5^2 f_6 \alpha^2 L^2}{f_4^2 f_7 g \beta \theta_w} 0.9^5 + \frac{5 \alpha^2 f_5 (2 f_1 f_5 + f_3 f_4 Pr)}{2 f_2 f_4^2 g \beta \theta_w} \left(L^2 - y^2 \right) \right]^{1/5} \\ &= \frac{L}{(Ra_L Pr)^{1/5}} \left[A - B \left(\frac{y}{L} \right)^2 \right]^{1/5} \end{aligned} \tag{15}$$

The coefficients A and B are

$$\begin{aligned} A &= 2 \times 0.9^5 \frac{f_5^2 f_6}{f_4^2 f_7} + B \\ B &= \frac{5}{2} \frac{f_5 (2 f_1 f_5 + f_3 f_4 Pr)}{f_2 f_4^2} \end{aligned} \tag{16}$$

A similar calculation of the boundary layer thickness at the critical point was performed previously [6], however somewhat differently. First, the calculation was carried out numerically, secondly, it was performed for a minimal fluid energy at the critical point, and thirdly, it accounted for a constant fluid density neglecting the effects of thermal expansion on the buoyancy and pressure components of the mechanical energy. Consequently, that approach produced a critical depth, which is 2.2 folds larger than the current prediction and thereby underestimated the heat flux. In contrast to the necessity of numerical calculations, the current solution is fully analytical and reveals in simple terms the variation of the boundary layer thickness across the strip. Furthermore, the current solution does account for effects of thermal expansion and buoyancy.

The local heat transfer coefficient and Nusselt number, for the temperature profile (4b), are

$$h_y = - \left. \frac{k \partial \theta}{\theta_w \partial z} \right|_{z=0} = \frac{f_5 k}{\delta} \tag{17a}$$

$$Nu_y = \frac{h_y y}{k} \tag{17b}$$

The average heat transfer coefficient, $\bar{h}$, is therefore

$$\begin{aligned} \bar{h} &= \frac{1}{L} \int_0^L h_y \, dy \\ &= \frac{f_5 k}{L} (Ra_L Pr)^{1/5} A^{-1/5} F \left(\frac{1}{5}, \frac{1}{2}; \frac{3}{2}; \frac{B}{A} \right) \end{aligned} \tag{18}$$

where $F(w, x; y; z)$ is the Gauss hypergeometric function defined by

$$F(w, x; y; z) = \frac{\Gamma(y)}{\Gamma(w)\Gamma(x)} \sum_{n=0}^{\infty} \frac{\Gamma(w+n)\Gamma(x+n)}{\Gamma(y+n)} \cdot \frac{z^n}{n!} \tag{19}$$

The corresponding averaged Nusselt number is

$$\overline{Nu}_L = \frac{\bar{h} L}{k} = \left[f_5 A^{-1/5} F \left(\frac{1}{5}, \frac{1}{2}; \frac{3}{2}; \frac{B}{A} \right) Pr^{1/5} \right] Ra_L^{1/5} \tag{20}$$

This expression is valid for any velocity and temperature profiles that are of the form of Eqs. (4a) and (4b), respectively.

3. Numerical solution

A numerical solution was obtained with the Icepak CFD code. In principle, the code solves the governing set of elliptic partial differential equations for conservation of mass, momentum and energy. The buoyancy forces representation is based on the Boussinesq approximation. The flow is, therefore, considered as essentially incompressible. The fluid properties are assumed constant and are evaluated at the average temperature between the hot surface and the ambient fluid. The solution is for conditions of steady-state laminar free convection.

Illustration of the boundaries used for the numerical model is presented in Fig. 3. The hot strip is located at the upper surface of the rectangular control volume and is isothermal. The size of the control volume was extended horizontally and vertically up to the point that it ceased to influence the calculated flow and temperature fields within the strip boundary layer. In particular, this applies to the dimensions "a" and "b" shown in the figure. The characteristic dimensions that were found as adequate are $a = 0.4L$ and $b = 2L$. Further extension of those dimensions does not entail any perceptible difference in the calculated heat transfer coefficient. Clearly, the ambient circulatory flow is seen as streamlines entering and leaving the control volume enclosure. At these free boundaries, according to the Icepak manual [12], viscosity effects are neglected, and the pressure is

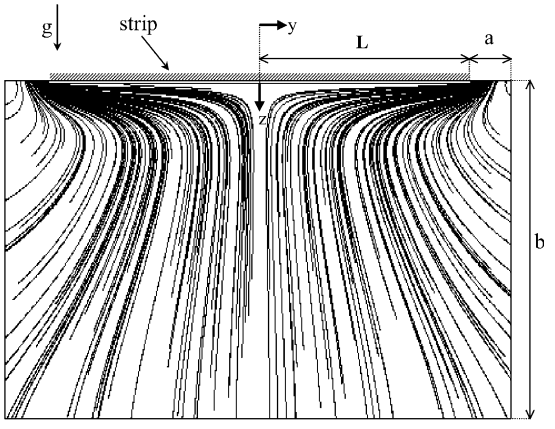

Fig. 3. Numerical simulation of streamlines underneath a hot strip ($\theta_w = 55.2$ °C, $Ra_L = 8.2 \times 10^6$).

assumed to be equal to the ambient pressure. Likewise, the flow entering the control volume is assumed to be at the ambient temperature.

To solve the problem, the code divides the flow domain into control volumes. The numerical scheme integrates the governing equations over each control-volume to construct a set of algebraic equations after linearization of the results. The set is then solved iteratively by the Gauss–Seidel linear equation solver for algebraic multigrid systems (AMG) until convergence is achieved. For convergence determination, the dimensionless residual term of each equation was calculated after each iteration. Convergence was achieved when the residual terms of the continuity and momentum equations were smaller than 10^{-3}, and smaller than 10^{-7} for the energy equation. Grid independence was obtained with cell numbers ranging from 80×50 to 80×400 for different strip widths. The verification was based on cutting by half the grid size and confirming that the heat transfer coefficient difference was smaller than 2%.

The computation results provided numerical velocity and temperature profiles. The numerical computation was verified by the successful reproduction of Aihara et al. [1] test results.

4. Results and discussion

Aihara et al. [1] measured the free convection velocity and temperature profiles underneath a hot horizontal surface facing down. Their test results were successfully reproduced by our numerical analyses. As seen in Fig. 3, the calculated stream lines indicate that far of the strip the flow moves upwards towards the strip center and as it approaches the strip it changes direction and moves towards its edges. The points of inversion form a virtual boundary that separates the boundary layer type flow from the external flow. In the literature, the flow confined between this virtual boundary and the strip surface has been indeed defined and considered as a boundary layer flow. The boundary layer thickness, at any location, is the distance between the strip and the point where the flow lacks any lateral velocity. A discrepancy was found between the experimental and calculated external flow streamlines. This is attributed to the arbitrary nature of the imposed conditions at the free control volume boundaries (chosen for numerical simulation convenience). However this discrepancy had no adverse effects on the boundary layer temperature and velocity numerical simulation. As most free convection problems, the boundary layer characteristics are primarily a function of the hot surface geometry and temperature difference, and are quite independent of the conditions that exist at a distance from the hot surface. To further elucidate this point, it is well accepted that problems of free convection along plates can be treated as parabolic problems. In reality these are elliptic problems. However the negligible inertia of the external flow is the reason why those problems can be treated as parabolic. Therefore, studies of the flow near the surface can be successfully conducted without any attempt to reproduce accurately the external circulatory flow. This explains why the inaccuracy of the external flow in the current study did not impair the results near the surface.

Calculated velocity profiles within the boundary layer are compared to experimental results [1] in Fig. 4a and b, for Raleigh numbers 8.2×10^6 and 1.17×10^7, corresponding to $\theta_w = 55.2$ and 104 °C, respectively. As seen, the velocity accelerates along the flow towards the strip edge and therefore the boundary layer thickness diminishes accordingly. Clearly, a good agreement exits between the measured and calculated results almost across the entire boundary layer along three different positions. The location of the maximum velocity is well reproduced. The discrepancy near the boundary layer edge stems from the approximate external flow calculations that yield flow streamlines of low curvature, entailing an imprecise definition of the flow inversion envelope (this also applies to the accuracy of the experimental measurements). However, this discrepancy hardly affects the calculated drag and overall inertia forces of the flow (that depend on the velocity gradient at $z = 0$ and the integral of the squared velocity profile, respectively). Furthermore, this discrepancy does not affect the calculated thermal energy transport rate. This is apparent in the successful numerical prediction of the experimental temperature profiles. Inspection of the temperature profiles seen in Fig. 5a and b, for Raleigh numbers 7.16×10^6 and 1.02×10^7 that corresponds to $\theta_w = 52.8$ and 101.1 °C, respectively, reveals an excellent agreement throughout the boundary layer zone. This applies to the thermal boundary layer thickness, δ_t. To further demonstrate the latter, the thermal boundary

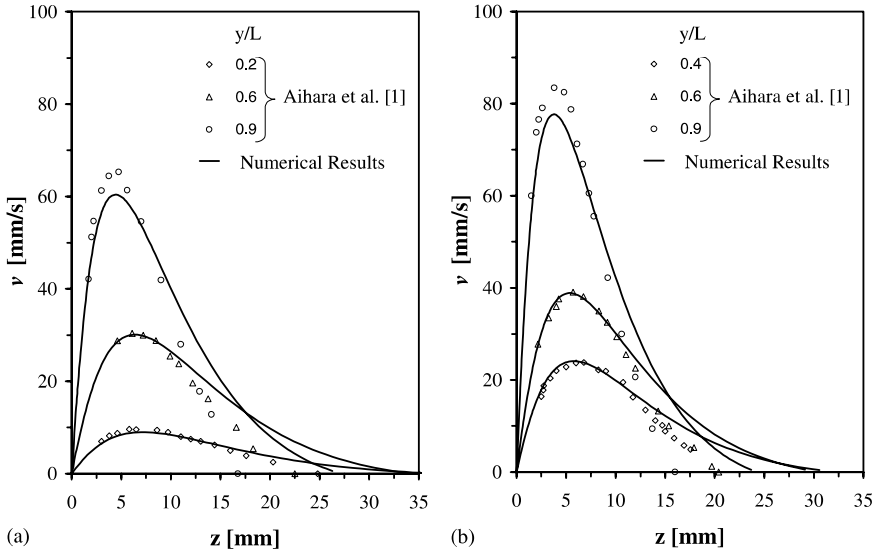

Fig. 4. Comparison between numerical and experimental velocity profiles underneath a hot surface. (a) $\theta_w = 55.2$ °C, $Ra_L = 8.2 \times 10^6$; (b) $\theta_w = 104$ °C, $Ra_L = 1.17 \times 10^7$.

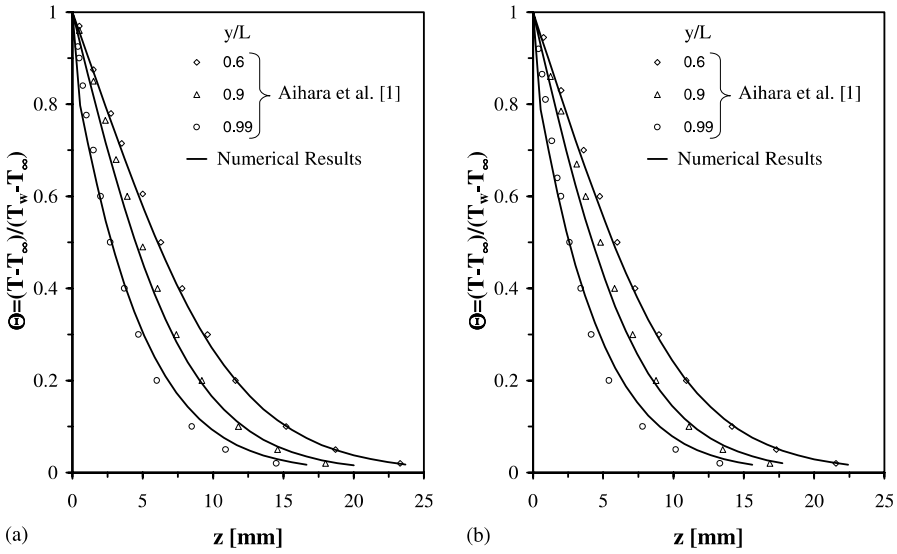

Fig. 5. Comparison between numerical and experimental temperature profiles underneath a hot surface. (a) $\theta_w = 52.8$ °C, $Ra_L = 7.16 \times 10^6$; (b) $\theta_w = 101.1$ °C, $Ra_L = 1.02 \times 10^7$.

layer thickness profiles are presented and compared in Fig. 6. Aihara et al. [1] assumed that the boundary layer extends up to the point where the temperature difference between the fluid and the surrounding air shrinks to 2% of θ_w. The small difference observed at the strip edge is of limited significance. It may result from, either or both, the somewhat arbitrary definition of the free boundaries of the numerical simulation control volume and the arbitrary (2%) definition of the measured boundary layer thickness. It is worth noting that the results presented in Fig. 6 are for two Raleigh numbers. The fact that the curves coincide, in their dimensionless form, indicates that for a given strip width, the boundary layer thickness is proportional to $Ra_L^{-1/5}$, as expected from theoretical analyses.

Dimensionless measured and calculated heat transfer coefficients, in terms of local Nusselt numbers (17b), are presented in Fig. 7. The results are in good agreement

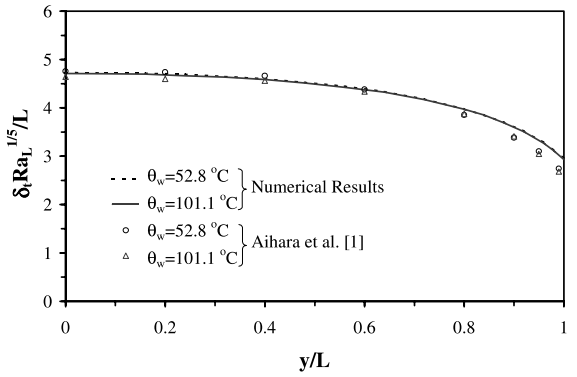

Fig. 6. Comparison between calculated and experimental dimensionless boundary layer thickness.

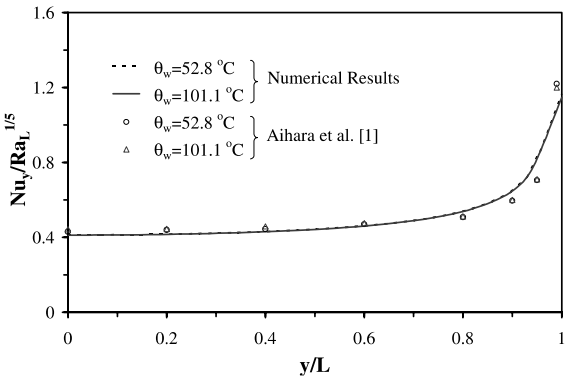

Fig. 7. Comparison between calculated and experimental local Nusselt numbers.

and indicate that the convective heat transport is strongest at the strip edge, where the boundary layer thickness is smallest. Averaged Nusselts' numbers over the strip width were calculated and found to coincide with Aihara et al. [1] results (with up to 2% difference, for the two Rayleigh numbers). Details of the comparison are presented in a later section. The remarkable reproduction of the experimental results, in effect, validates the accuracy of the numerical model.

The assumption that the hydrodynamic and temperature profiles exhibit similarity characteristics was justified numerically. Inspection of the numerically calculated velocity and temperature profiles of Fig. 8a and b reveals that fact. It is seen that the normalized velocity and temperature profiles stay constant along most of the flow course. For this strip width, small deviations from similarity exist only in the last 20% of the flow course (for larger strip, numerical analysis showed that the similarity deviations zone would be percentage wise smaller). Notice that the velocity profiles were normalized versus the boundary layer thickness rather than the location of the maximum velocity (the latter used by Aihara et al. [1]). The latter choice introduces a division by smaller numbers that unnecessarily amplify even tiny deviation form similarity, and should be avoided. To elucidate that point, assume that the mean location of the maximum velocity is roughly at 0.2δ. A deviation of 0.01δ (reflecting a 5% deviation) from that location is in

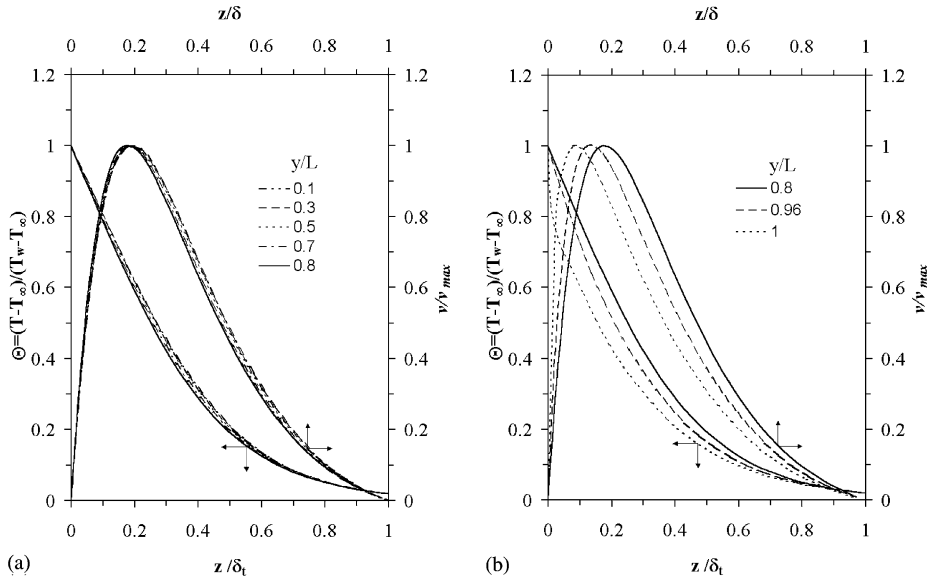

Fig. 8. Numerical calculation of normalized velocity and temperature profiles. (a) At various locations along 80% of the strip width; (b) at various locations along 20% of the strip width, near its edge.

effect inconsequential in terms of similarity considerations. However, if the profile is normalized according to 0.2δ, it would entail a deviation of 0.05δ at δ, which is significantly more noticeable. If Aihara et al. [1] experimental results were normalized versus their local inversion layer thickness, they would indeed exhibit similarity characteristics along most of the flow course. Obviously, Aihara's claim that similarity does not exist is not fully accurate. Similar arguments can be applied to the normalization technique of the temperature profiles, where the normalization is versus a fraction of δ, and thereby entails an unnecessary amplification effect.

In accordance with the above conclusions, several velocity and temperature profiles were examined for subsequent incorporation in the integral solution method. Polynomial of different orders, that satisfy the boundary conditions, described in Eqs. (3a) and (3b), turned out to produce small differences in their results. Consequently, the most commonly used profiles for natural convection analytical investigation were incorporated in our analyses. The velocity and temperature profiles are therefore:

$$\frac{v}{V} = \eta(1-\eta)^2 \tag{21a}$$

$$\frac{T-T_\infty}{T_w-T_\infty} = \frac{\theta}{\theta_w} = (1-\eta)^2 \tag{21b}$$

A comparison of these profiles with those measured by Aihara et al. [1] is shown in Fig. 9a and b. As previously mentioned, similarity prevails more at the strip central region and less near its edges.

Substitution of the velocity and temperature profile, Eqs. (21a) and (21b), into Eq. (16) yields the following boundary layer thickness equation

$$\delta = \frac{L}{(Ra_L Pr)^{1/5}}\left[A - B\left(\frac{y}{L}\right)^2\right]^{1/5} \tag{22}$$

The coefficients A and B are

$$\begin{aligned} A &= 1173.5 + 900Pr \\ B &= 128.57(8 + 7Pr) \end{aligned} \tag{23}$$

and based on Eq. (20)

$$\overline{Nu}_L = \frac{\bar{h}L}{k} = CRa_L^{1/5} \tag{24}$$

where $C = 0.462$ (for $Pr = 0.7$).

As mentioned in the Section 1, a noticeable discrepancy exists in the published values of the coefficient C. A search for the reason for this discrepancy revealed that it could be attributed to the fact that previous investigations were conducted for different strip widths. Inspection of Fig. 8b reveals that the similarity assumption does not fully apply near the strip edge. In this region, vertical flow vector components and gravitational forces are influencing. The strip edge effects have a resemblance to entrance effects in pipe flow. The relative importance of these edge effects is more pronounced at narrower strips. To verify this point, we conducted numerical calculations for various strip widths and plotted the results in Fig. 10. The choice of the dimensionless parameter (L^*) against which the curve is plotted in the figure emanates from dimensionless analysis of the

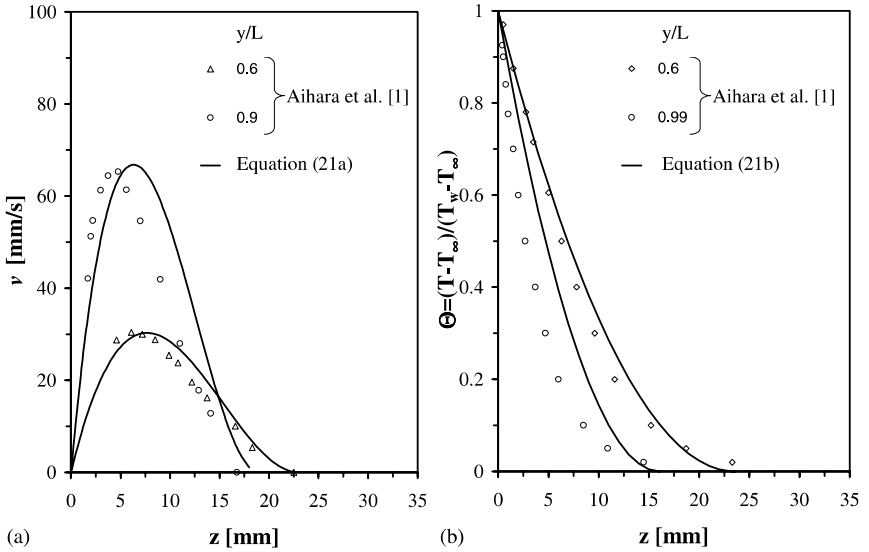

Fig. 9. Comparison between calculated and experimental profiles underneath a hot surface. (a) Velocity profiles ($\theta_w = 55.2$ °C, $Ra_L = 8.2 \times 10^6$). (b) Temperature profiles ($\theta_w = 52.8$ °C, $Ra_L = 7.16 \times 10^6$).

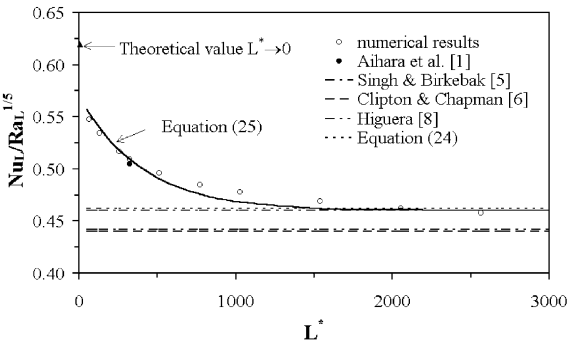

Fig. 10. Effect of strip width on the average Nusselt number (for $Pr = 0.7$).

momentum equation in the vertical direction. Therefore, this parameter constitutes a natural choice for the characterization of the relative importance of the edge region relative to the entire strip width. Notice that this parameter is not temperature dependent and is of significance only for narrow strips.

The general trend is one of higher heat transfer coefficients for narrower strips. This, in principle, stems from edge effects that substantially increase the local heat transfer rates and thereby the averaged Nu numbers of narrower strips. Indeed, Aihara experimental coefficient C seems to perfectly fit the numerical simulation results, as seen in Fig. 10. Likewise, Goldstein and Lau [7] calculated the value of C for small Rayleigh numbers, which indeed is greater than those of large strips. Other investigations of Singh and Birkebak [5], Clifton and Chapman [6] and Higuera [8], as well as the present analytical solution, were developed for large strip widths and consequently better fit our numerical results for those widths. It is expected that the value of C would diminish and approach asymptotically the value of very large strips. In this context, but for the opposite limit, one may assume that for a very narrow strip the boundary layer thickness roughly equals its critical value. Accordingly, by plugging the critical δ_C, Eq. (14), into the Nusselt number, Eqs. (17a) and (17b), one gets a theoretical value of $C = 0.62$, which seems to represent a point that resides close to a smooth extension of the C curve in Fig. 10. The forgoing arguments call for a modified formulation of the Nusselt number, which should account for the added dependence on the strip width. The new representation is semi-empirical and was developed to fit the numerical results. The correlation is of a simple exponential form and is

$$\overline{Nu}_{\mathrm{L}} = C(L^*)Ra_{\mathrm{L}}^{1/5} \tag{25}$$

where

$$C(L^*) = 0.46[1 + 0.24\exp(-0.0025L^*)]$$

and

$$L^* = \frac{L}{\sqrt[3]{\alpha\nu/g}}$$

The dimensionless length L^* is based on a group of properties that reflect the boundary layer thickness which tends to increase with α and ν, and decreases with g. Notice that the above conclusions shed new light on an important aspect of strip natural heat transport characteristics. It is important to point out that the correlation accommodates the predicted value of C as $L \to \infty$. It also fits the experimental data point of Aihara [1], and comes close to the approximate value for the limiting case of $L \to 0$. An error estimate of the correlation accuracy that accounts also for Aihara's experiments error is $\pm 5\%$.

5. Conclusions

An analytical study was conducted to develop a closed form solution for the natural convection heat transfer coefficient underneath an isothermal horizontal hot strip. The contribution of the study is summarized as follows:

- It is demonstrated numerically that the boundary layer can be assumed to have similarity characteristics along most of the strip width. It is also shown that a proper inspection of experimental data can lead to the same conclusion.
- The present study has an advantage over previous investigations because it provides, first, a fully analytical solution, second, it accounts for inertia effects on top of all other effects, and third, it is based on a more comprehensive critical flow representation at the strip edge.
- The current analyses explain why a discrepancy exists amongst published correlations. It goes further to show that an added dimensionless parameter must be accounted for so that the Nusselt number would apply to narrow strip widths.

The results were successfully tested against existing experimental results. The analytical approach of the present investigation can be applied for the solution of more complex natural convection problems.

References

[1] T. Aihara, Y. Yamada, S. Endo, Free convection along the downward facing surface of a heated horizontal plate, Int. J. Heat Mass Transfer 15 (1972) 2535–2549.

[2] T. Fujii, H. Imura, Natural-convection heat transfer from a plate with arbitrary inclination, Int. J. Heat Mass Transfer 15 (1972) 755–767.

[3] C. Wagner, Discussion on integral method in natural convection flow, J. Appl. Mech. 23 (1956) 320–321.
[4] S.N. Singh, R.C. Birkebak, R.M. Drake, Laminar free convection heat transfer from downward-facing horizontal surfaces of finite dimensions, Prog. Heat Mass Transfer 2 (1969) 87–98.
[5] S.N. Singh, R.C. Birkebak, Laminar free convection from a horizontal infinite strip facing downwards, ZAMP 20 (1969) 454–461.
[6] J.V. Clifton, A.J. Chapman, Natural convection on a finite size horizontal plate, Int. J. Heat Mass Transfer 12 (1969) 1573–1584.
[7] R.J. Goldstein, K.S. Lau, Laminar natural convection from a horizontal plate and the influence of plate-edge extensions, J. Fluid Mech. 129 (1983) 55–75.
[8] F.J. Higuera, Natural convection below a downward facing horizontal plate, Eur. J. Mech. B Fluids 12 (1993) 289–311.
[9] D.W. Hatfield, D.K. Edwards, Edge and aspect ration effects on natural convection from the horizontal heated plate facing downwards, Int. J. Heat Mass Transfer 24 (6) (1981) 1019–1024.
[10] R.L. Daugherty, J.B. Franzini, in: Fluid Mechanics with Engineering Applications, seventh ed., McGraw-Hill, New York, 1977, pp. 334–337.
[11] M. Sadatom, M. Kawaji, C.M. Lorencez, T. Chang, Prediction of liquid level distribution in horizontal gas–liquid stratified flows with interfacial level gradient, Int. J. Multiphase Flow 19 (6) (1993) 987–997.
[12] Fluent Inc., Icepak 3 User's Guide, 1999.